ACS OMEGA

http://pubs.acs.org/journal/acsodf

Article

Ni Nanocrystals Supported on Graphene Oxide: Antibacterial Agents for Synergistic Treatment of Bacterial Infections

Ting Du,[‖] Baojia Huang,[‖] Jiangli Cao, Chunqiao Li, Jingbo Jiao, Zehui Xiao, Lifei Wei, Jing Ma, Xinjun Du,* and Shuo Wang*

Cite This: *ACS Omega* 2022, 7, 18339−18349

Read Online

ACCESS | Metrics & More | Article Recommendations | Supporting Information

ABSTRACT: The effects of antibiotics on bacterial infections are gradually weakened, leading to the wide development of nanoparticle-based antibacterial agents with unique physical and chemical properties and antibacterial mechanisms different from antibiotics. In this study, we fabricated the uniform and stable graphene oxide (GO)/Ni colloidal nanocrystal cluster (NCNC) nanocomposite by electrostatic self-assembly and investigated its synergistic antibacterial activity against *Staphylococcus aureus* (*S. aureus*) and *Escherichia coli* (*E. coli*) in vitro. The GO/NCNC nanocomposite was shown to possess higher inhibition efficiency than a pure NCNC or GO suspension, with 99.5 and 100% inhibition against *S. aureus* and *E. coli* at a 125 μg/mL concentration, respectively. Antibacterial mechanism analysis revealed that (i) NCNCs decorated on GO can further enhance the antibacterial properties of GO by binding and capturing bacteria, (ii) the leaching of Ni^{2+} was detected during the interaction of GO/NCNCs and bacteria, resulting in a decrease in the number of bacteria, and (iii) the GO/NCNC nanocomposite can synergistically destroy the bacterial membrane through physical action and induce the reactive oxygen species generation, so as to further damage the cell membrane and affect ATPase, leakage of intercellular contents, and ultimately bacterial growth inhibition. Meanwhile, cell culture experiments demonstrated no adverse effect of GO/NCNCs on cell growth. These preliminary results indicate the high antibacterial efficiency of the GO/NCNC nanocomposite, suggesting the possibility to develop it into an effective antibacterial agent in the future against bacterial infections.

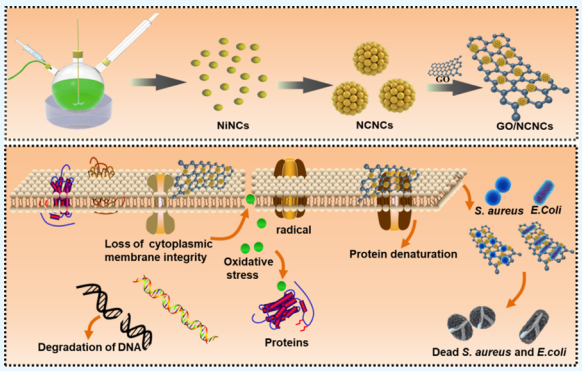

1. INTRODUCTION

Pathogenic bacterial infections with high morbidity and mortality are one of the most serious health problems that have caused worldwide concern, and the use of antibiotics is a traditional treatment strategy to effectively reduce deaths caused by bacterial infections.[1] However, the occurrence of drug-resistant strains and biofilm pathogenic cells [which are usually embedded in different types of biopolymers, called extracellular polymeric substances (EPSs)][2] has become an important factor affecting the therapeutic effects of antibiotics; especially, EPSs may prevent the contact of antibacterial agents with bacteria.[3] At present, the commonly used clinical strategy to improve the therapeutic effect is increasing the dose of antibiotics, which may cause more serious side effects and accelerate the development of drug-resistant strains. It is very necessary to develop new antibacterial agents with good biosafety and excellent antibacterial activity.

In this regard, researchers have investigated various antibacterial materials, such as metal-based nanoparticles (NPs) (Ag-based, Au-based, ZnO-based, and Cu-based),[4−9] carbon-based NPs (CDs, GO, and CNTs),[10,11] cationic polymers,[12,13] antimicrobial peptides,[14] hydrogels,[15−17] and magnetic NPs.[18−20] These antibacterial materials have exhibited excellent antibacterial properties in the control and prevention of drug-resistant bacterial infections, especially magnetic NPs. They are considered as an effective tool against pathogenic biofilms and have important applications as nanocarriers in drug delivery. However, in order to endow magnetic NPs with these properties, it is necessary to functionalize their surface with proteins, or other nano-components, and then apply a magnetic field to guide the agents into the biofilm, destroy it, or achieve magnetic separation of bacteria.[21,22] This suggests that it is a challenge to prepare functional entities connecting magnetic NPs and bacteria.

In 2018, superparamagnetic Ni colloidal nanocrystal clusters (NCNCs) were reported for the first time as a novel type of

Received: January 25, 2022
Accepted: May 12, 2022
Published: May 24, 2022

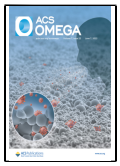

Scheme 1. Schematic Illustration of Preparation of the GO/NCNC Nanocomposite and the Corresponding Antibacterial Application

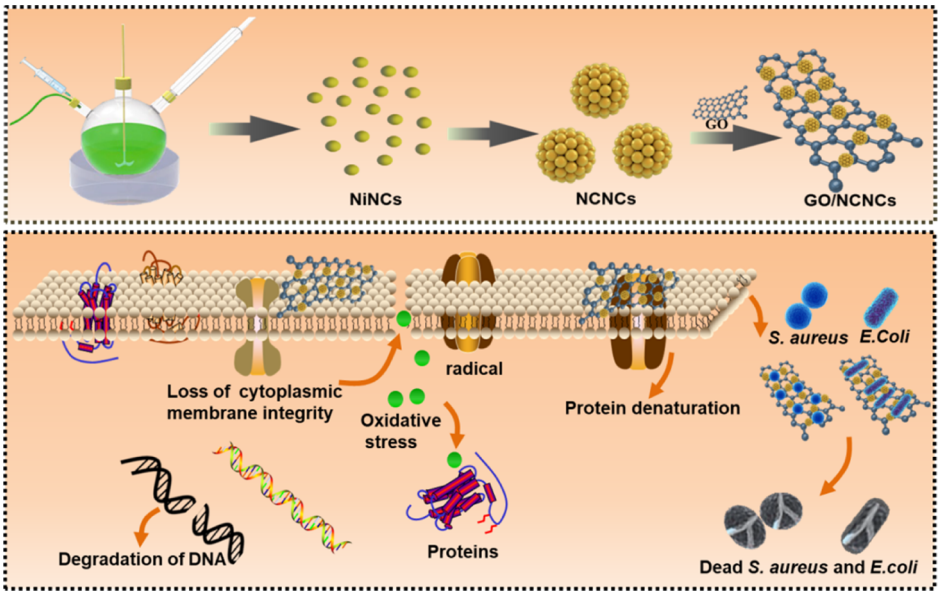

magnetic material with antibacterial and binding characteristics against Gram-positive/-negative bacteria and bacterial spores.[23] To date, the mechanism for the antibacterial effect of NCNCs is still not fully understood, and most magnetic materials have the disadvantage of easy agglomeration. Additionally, several researchers have pointed out that for many complex bacterial infections, single-agent treatment and single-mode antibacterial technology can hardly achieve the purpose of effective eradication of bacteria.[24] Therefore, the present study aimed to synthesize a magnetic nanocomposite with good dispersion and efficient removal of bacteria.

Graphene oxide (GO) is a two-dimensional sheet material with single-atom thickness, which has large specific surface area and good water dispersibility.[25] The presence of hydroxyl, carboxyl, and epoxy groups on the surface makes it easy to be chemically modified, and it has proved to be an excellent carrier material.[26] Besides, a variety of GO-based components confirmed to be potent antimicrobials with low cytotoxicity and broad-spectrum antimicrobial activity.[27] For example, GO can exert antibacterial and antifungal activities by directly acting on bacteria or spore membranes and causing physical damage.[28] A GO−AgNP nanocomposite showed enhanced antimicrobial activity against the phytopathogen *Fusarium graminearum*.[29] Liang et al. prepared a biocompatible antibacterial nano-platform by embedding a thin-layer GO sheet loaded with zinc oxide quantum dots into the hydrogel, and the composite material was shown to have good antibacterial efficacy.[30] However, there is no research about the preparation of nanocomposites using GO as a carrier of NCNCs for antibacterial application.

In this study, the GO-decorated NCNC (GO/NCNC) antibacterial nanomaterial was developed for synergistic antibacterial therapy. The NCNCs can magnetically bind and capture bacteria, and the addition of GO as a carrier improves the biocompatibility and dispersibility of NCNCs, in addition to synergistically enhancing the antibacterial activity. *In vitro* experiments showed that the GO/NCNC nanocomposite has stronger antibacterial activity than pure NCNCs and GO, suggesting that the GO/NCNC nanocomposite has great potential in inhibiting bacterial infections (Scheme 1).

2. EXPERIMENTAL SECTION

2.1. Reagents and Materials. In this work, diethylene glycol (DEG, ≥99.0%) and polyethyleneimine (PEI) were purchased from Sigma-Aldrich (China); nickel(II)chloride ($NiCl_2$, ≥99.0%) and sodium citrate tribasic dehydrate (NaCit, ≥99.0%) from Macklin Chemistry Co. Ltd. (Shanghai, China); and sodium hydroxide pellets (NaOH, ≥96%) from Tianjin Jiangtian Chemical Technology Co., Ltd. (Tianjin, China). The *Staphylococcus aureus* (*S. aureus*) (ATCC 26003) and *Escherichia coli* (*E. coli*) (ATCC 700927) were provided by our laboratory.

2.2. Synthesis of Magnetic NCNCs. The NCNCs were prepared using a slightly modified previously reported method.[23] Briefly, NaOH (15 mM) was dissolved in 6.0 mL of DEG and stirred at 150 °C until complete dissolution, followed by storing the resultant light-yellow transparent solution at 4 °C before further use. Next, a mixture consisting of 4.0 mM $NiCl_2$, 1.7 mM NaCit, and 20 mL of DEG was mechanically stirred at 200 rpm and 200 °C for 30 min in a N_2 atmosphere. Subsequently, the as-prepared NaOH/DEG mixture was quickly added to the $NiCl_2$/NaCit/DEG phase, and the color changed rapidly from green to black, followed by 2 h of reaction and naturally cooling the mixture to room temperature. After purifying the obtained magnetic NCNCs by two washes with ethanol and three washes with water, the obtained NCNCs were freeze-dried into powder and stored at 4 °C before further use.

2.3. Preparation of the GO/NCNC Nanocomposite. The GO/NCNC nanocomposite was prepared via electrostatic self-assembly. Briefly, the GO was exfoliated via ultrasonic treatment in deionized water for 2 h to acquire uniformly dispersed GO solution (1.0 mg/mL). Meanwhile, PEI-capped NCNCs were synthesized by mixing 10 mg of NCNCs with 3.0 mg/mL PEI solution and stirring for 1 h; the resulting mixture was washed three times by centrifugation to remove excess PEI and then resuspended in 1.0 mL of deionized water.

https://doi.org/10.1021/acsomega.2c00508
ACS Omega 2022, 7, 18339−18349

Next, 1.0 mg/mL GO was added to 10 mg of PEI-capped NCNCs for self-assembly at 25 °C and 200 rpm for 24 h. Finally, the resultant GO/NCNC nanocomposite was washed by centrifugation and resuspended in deionized water.

2.4. In Vitro Antibacterial Test. Antibacterial activity of samples tested with *S. aureus* and *E. coli* as a model bacterium and the antibacterial activity of GO, NCNCs, and GO/NCNCs were measured using the growth curve method, agar plate method, minimal inhibitory concentrations (MICs), and live/dead staining as described below.

For the agar plate test, 100 μL (10^7 CFU/mL) of a bacterial suspension was cultured at 37 °C for 2 h with GO/NCNCs (GO or NCNCs) at different concentrations (250, 125, 62.5, 31.3, 15.6, and 7.80 μg/mL), with the control sample composed of 100 μL of the bacterial suspension and 100 μL of deionized water. Each group was divided into two parts, one for agar plate assay and the other for growth curve assay. After 2 h of treatment, 50 μL of bacterial dilution was spread onto the Luria−Bertani (LB) agar plate to count the number of colonies (CFUs) and then obtain the antibacterial rate by using the following equation

$$\text{antibacterial rate (\%)} = \left(1 - \frac{\text{CFU(experimental group)}}{\text{CFU(control group)}}\right) \times 100\% \quad (1)$$

For the growth curve test, the mixture in the other tube was transferred to 10 mL of LB broth, and the *S. aureus* samples were cultured in an incubator (37 °C) under continuous agitation at 200 rpm. The same amount of bacterial solution was taken from each group every 1 h, the optical density (OD) values at a 600 nm wavelength were tested, and the growth curve of *S. aureus* was drawn.

For the MIC test, 100 μL of log-phase bacterial solution was incubated with different concentrations of GO/NCNCs at 37 °C for 2 h, and the final concentrations of GO/NCNCs were 250, 125, 62.5, 31.3, 15.6, and 7.80 μg/mL. The above-mentioned co-incubation system (200 μL) was then added to 9.8 mL of LB liquid medium and incubated on a shaker (37 °C, 200 rpm/mL) for 18 h. The MIC value is defined as the minimum concentration of GO/NCNCs at which the bacterial growth is obviously inhibited compared to the blank, that is, the treatment concentration of the GO/NCNCs at which the solution is clear and free of bacterial growth.

For bacterial live/dead staining, the bacterial solution (10^7 CFU/mL) and GO/NCNCs (125 μg/mL) were co-incubated at 37 °C for 2 h, and then, we collected the bacterial solution through centrifugation, staining with propidium iodide (PI, 10 μg/mL) for 10 min, followed by 40-6-diamidino-2-phenylindole (DAPI, 5.0 μg/mL) for 5 min, with PI staining for dead bacteria (red) and DAPI staining for live bacteria (blue). After washing the samples twice with phosphate buffered saline (PBS), the survival and death of bacteria were recorded through an inverted fluorescence microscope (Nikon, Eclipse Ti-S).

2.5. Morphological Analysis of Bacterial Cells. In order to investigate the morphological changes of the bacteria in the presence or absence of GO, NCNCs, and GO/NCNCs (125 μg/mL), the bacteria were treated as described in Section 2.4. After fixation with 2.5% glutaraldehyde overnight, gradient dehydration was carried out for 15 min with ethanol concentrations of 30, 50, 70, 90, and 100%. The morphology of *S. aureus* was collected through high-resolution transmission electron microscopy (TEM) and scanning electron microscopy (SEM).

2.6. ROS Assay. The reactive oxygen species (ROS) generation in *S. aureus* cells exposed to GO, NCNCs, and GO/NCNCs was monitored by using 2′,7′-dichlorodihydrofluorescein diacetate fluorogenic (DCFH-DA) dye. First, *S. aureus* (10^7 CFU/mL) was exposed separately to GO, NCNCs, and GO/NCNCs (125 μg/mL) at 37 °C for 2 h; then, cells were rinsed in PBS and incubated with DCFH-DA (10 μM) at 37 °C for 1 h. After centrifugation at 5000 rpm for 5 min and three washes with PBS, the ROS level in the cells was examined with an inverted microscope.

2.7. Statistical Analysis. The experiments were conducted in triplicate and repeated three times. Data were processed using Origin Pro8 (OriginLab, Northampton, MA, USA) and shown as means ± standard deviation. *, **, ***, and **** indicate $p < 0.05$, <0.01, <0.001, and <0.0001 compared to the control group, respectively.

3. RESULTS AND DISCUSSION

3.1. Characterization of the GO/NCNC Nanocomposite. The GO/NCNC nanocomposite was prepared through electrostatic interaction. Specifically, GO and NCNCs were prepared separately, followed by using PEI as a surfactant to modify NCNCs and obtain positive potential functionalized NCNCs (PEI@NCNCs). Finally, the GO/NCNC nanocomposite was prepared by decorating negatively charged GO onto the surface of PEI@NCNCs under stirring. Figures 1a−d and S1 show the morphologies of NCNC, PEI@NCNC, GO, and GO/NCNC nanocomposites and the magnetic enrichment characteristics of the GO/NCNC nanocomposite. As illustrated in Figure S1a, the magnetization saturation (M_s) value of GO/NCNCs measured was 122.5 emu/g, indicating that GO/NCNCs are strong magnetic materials and sufficient for magnetic enrichment. In Figure 1d, the monodispersed NCNCs are seen to be uniformly decorated on the surface of the GO nanosheets, and the lattice spacing of the NCNCs is 0.11 nm (the illustration in the lower right corner). The UV−vis absorption spectra of NCNCs, GO, and GO/NCNCs are shown in Figure 1e. GO had a characteristic absorption peak at 228 nm ($\pi \rightarrow \pi^*$) and a shoulder peak at 300 nm ($n \rightarrow \pi^*$),[31] and NCNCs had no obvious characteristic absorption peaks.[23] The GO/NCNCs had a typical absorption peak at 215 nm, which was slightly blue-shifted compared with pure GO, and had a red-shifted absorption peak at 330 nm, demonstrating that the decoration of NCNCs on the GO surface is successful. Additionally, the electrostatic interaction between NCNCs and GO was further investigated (Figure 1f). The zeta potential of NCNCs was −10 ± 2.0 mV, and the value changed from negative to positive after PEI modification, suggesting the formation of positively charged PEI-NCNCs (21 ± 0.9 mV), which was conducive to the adsorption of negatively charged GO (−15 ± 5.1 mV) and the formation of the GO/NCNC nanocomposite with a zeta potential value of −9.9 ± 4.2 mV. The above-mentioned results proved that the GO/NCNC nanocomposite was successfully prepared.

In addition, the surface properties and crystalline structures of GO, NCNCs, and GO/NCNCs were characterized. As illustrated in Figure 2a, the peak located at 3250 cm^{-1} was the tensile vibration of O−H, and the absorption peaks at 2929, 1471, and 1078 cm^{-1} were attributed to the stretching and bending vibrations of C−H in the alkyl. Meanwhile, the peak at 1628 and 1380 cm^{-1} was due to the stretching vibrations of

https://doi.org/10.1021/acsomega.2c00508
ACS Omega 2022, 7, 18339−18349

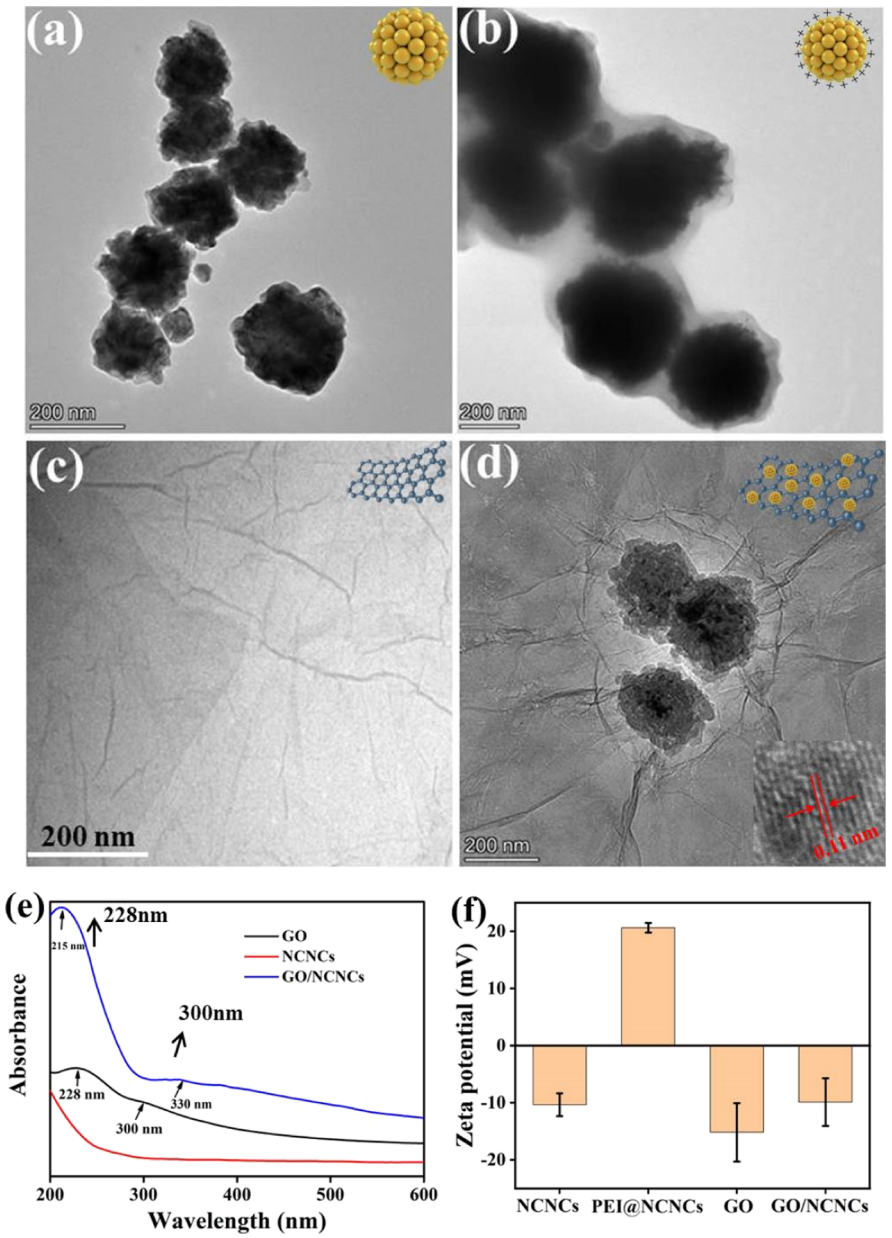

Figure 1. TEM images of NCNCs (a), PEI@NCNCs (b), GO (c), and GO/NCNCs (d). UV−vis absorption (e) and zeta potentials (f) of GO, NCNCs, and GO/NCNCs.

C═O and C−O, respectively. These absorption peaks indicated that NCNCs were decorated on GO nanosheets.[23,32] As shown in Figure 2b, the characteristic peak of GO at 10.5° was ascribed to the (001) reflection plane of GO,[33] and the three typical diffraction peaks of NCNCs at 44.5, 58.4, and 78.0° corresponded to the (011), (012), and (103) crystal planes (PDF #45-1027), respectively, proving the successful synthesis of NCNCs,[23] whereas the characteristic peaks of GO at 9.5° and NCNCs at 44.7° appeared after NCNCs were decorated on GO. This result further indicated the successful preparation of the nanocomposite.

The chemical states of GO (Figure S2), NCNCs (Figure S3), and GO/NCNCs (Figure 2c−f) were measured by X-ray photoelectron spectroscopy (XPS). Figure 2c shows the XPS survey spectrum of GO/NCNCs showing the presence of Ni, O, and C elements. In Figure 2d, Ni 2p is seen to contain three peaks at 856.88, 860.28, and 863.83 eV, assigned to Ni ($2p_{3/2(b)}$), Ni (2p sat), and Ni ($2p_{1/2(a)}$), respectively. Figure 2e is the C 1s XPS spectrum showing the sharp peaks at 285.18 eV and 287.48 eV ascribed to the C−C and epoxy groups, respectively. The O 1s peak at 532.11 eV might indicate the existence of oxygen in the form of C−OH/C−O−C (Figure 2f). These observations are consistent with a previous study.[34]

3.2. Cytotoxicity. Biocompatibility is a prerequisite for in vivo application of nanomaterials. In this study, the biotoxicity of GO/NCNCs, GO, and NCNCs on the viability of Vero cells was tested via the 3-(4,5-dimethylthiazol-2-yl)-2,5-diphenyltetrazolium bromide (MTT) method. In Figure 3, incubation of Vero cells with different concentrations of GO/NCNCs, GO, and NCNCs is shown to have a cell viability above 85% within the concentration range of 62.5 μg/mL to 0.25 mg/mL, indicating the biocompatibility of GO/NCNCs.

3.3. In Vitro Antibacterial Activity. The antibacterial capability of GO/NCNCs, GO, and NCNCs against *S. aureus*

https://doi.org/10.1021/acsomega.2c00508
ACS Omega 2022, 7, 18339−18349

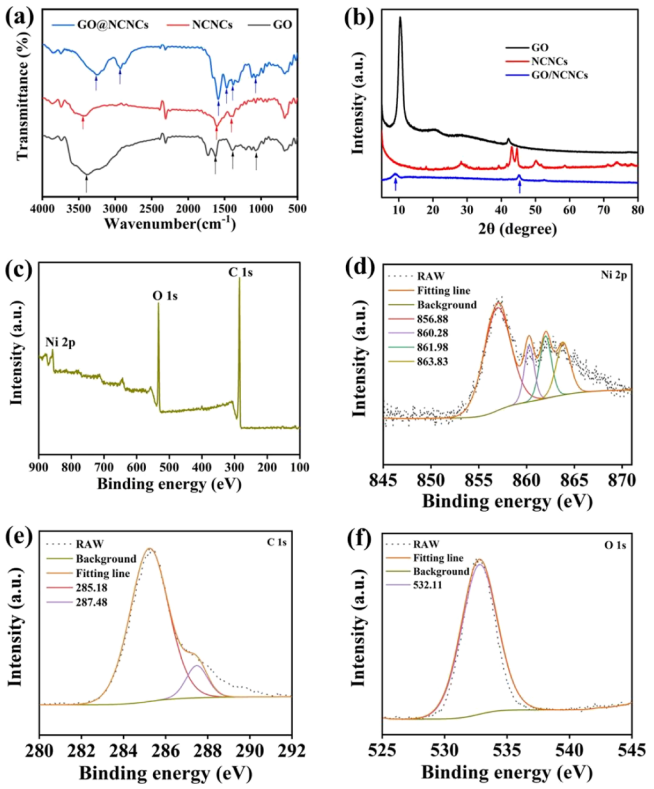

Figure 2. FT-IR spectra (a) and XRD patterns (b) of GO, NCNCs, and GO/NCNCs. XPS survey spectra of GO/NCNCs: overall spectrum (c), Ni 2p (d), C 1s (e), and O 1s (f).

was evaluated by the agar plate experiment *via* comparison of the survival rate of *S. aureus*, and the results are displayed in Figure 4. After the control group was cultured in a 37 °C incubator, plentiful of viable colonies emerged on the plates, while the treatment with GO, NCNCs, and GO/NCNCs showed a gradual dose-dependent decrease in the number of colonies (7.8−250 μg/mL) (Figure 4d). Compared with the control group, the GO group displayed significant reduction in the number of colonies, with an antibacterial rate of 82% at a concentration of 125 μg/mL (Figure 4b). Previous research has attributed the excellent antibacterial ability of GO to its unique layer structure and photochemical properties.[35−37] The NCNC group also showed a decrease in the number of colonies, with an antibacterial rate of 70.8% at 125 μg/mL (Figure 4c). Previous studies have shown that NCNCs could exhibit obviously antibacterial and trapping ability against both Gram-positive/-negative bacteria and bacterial spores.[23] Notably, in Figure 4a, GO/NCNCs are shown to have killed 99.5% *S. aureus* at 125 μg/mL, indicating the successful construction of the GO/NCNC synergetic antibacterial system.

Additionally, using *E. coli* as the model bacterium of Gram-negative bacteria, the inhibitory effect of different concentrations of GO/NCNCs, GO, and NCNCs on *E. coli* was investigated. As illustrated in Figure S4, compared with the control group, the inhibitory effect of the material treatment group was positively correlated with the material concentration. When the concentration was 125 μg/mL, the number of colonies in the GO treatment group, the NCNC treatment group, and the GO/NCNC treatment group was significantly reduced, and the inhibition efficiencies were 99.7, 99.8, and 100%, respectively. This result is consistent with the inhibition of *S. aureus*, indicating that the GO/NCNCs have strong antibacterial activity.

To further quantitatively study the antibacterial effects of the GO/NCNCs, GO, and NCNCs, the MICs of *S. aureus* and *E. coli* exposed to GO/NCNCs, GO, and NCNCs were measured. As displayed in Table S1, the MIC of GO/NCNCs against *S. aureus* and *E. coli* was 125 and 62.5 μg/mL, respectively, which was higher than that of pure GO and NCNCs, suggesting that GO/NCNCs have stronger antibacterial activity against *E. coli* than against *S. aureus*.

The antibacterial efficiency of GO/NCNC nanocomposites was further explored through analyzing the growth curve and live/dead fluorescence experiments. *S. aureus* was cultured in LB medium, and samples were taken at different culture time points to detect the optical density at OD_{600nm}. As shown in Figure 5a, GO/NCNCs could obviously inhibit the growth of *S. aureus* in the concentration range of 7.80 to 250 μg/mL. Similarly, as shown in Figure 5b, the *S. aureus* treated with 125 μg/mL GO/NCNCs showed a large amount of red fluorescence, and almost no blue fluorescence was observed, suggesting that most of *S. aureus* cells were dead. Inversely, the control group presented blue fluorescence emission without red spots, demonstrating that abundant *S. aureus* cells were alive. The aforementioned results were corroborated by the agar plate assay, indicating that the GO/NCNC nanocomposite has an excellent antibacterial effect.

3.4. Antibacterial Mechanism. *3.4.1. Changes in the Cell Structure Induced by GO/NCNCs.* The cell membrane, a barrier to protect bacteria from harmful substances, is basis for maintaining the basic functions of bacteria. The direct interaction of GO with a pathogen will cause the pathogen

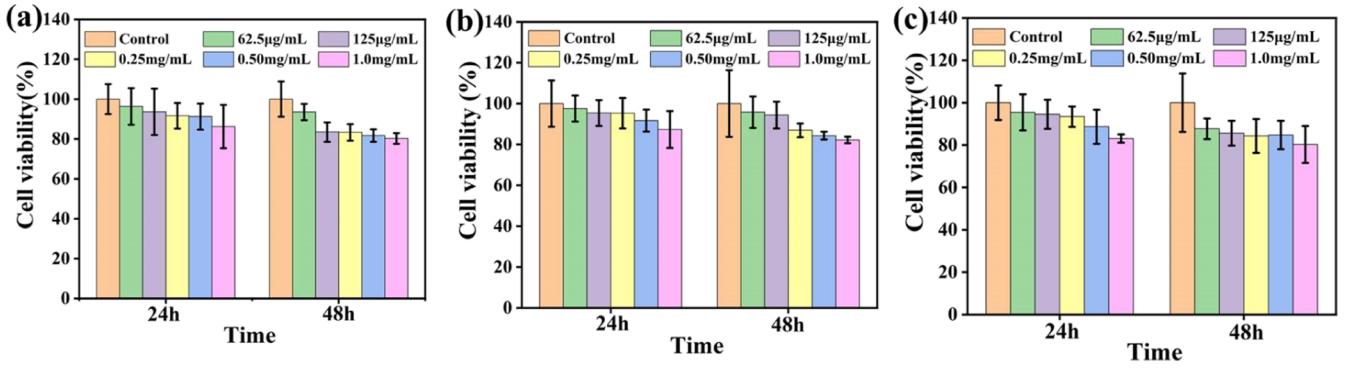

Figure 3. Effects of different concentrations of GO/NCNCs (a), GO (b), and NCNCs (c) on the Vero cell viability investigated by the MTT assay.

https://doi.org/10.1021/acsomega.2c00508
ACS Omega 2022, 7, 18339−18349

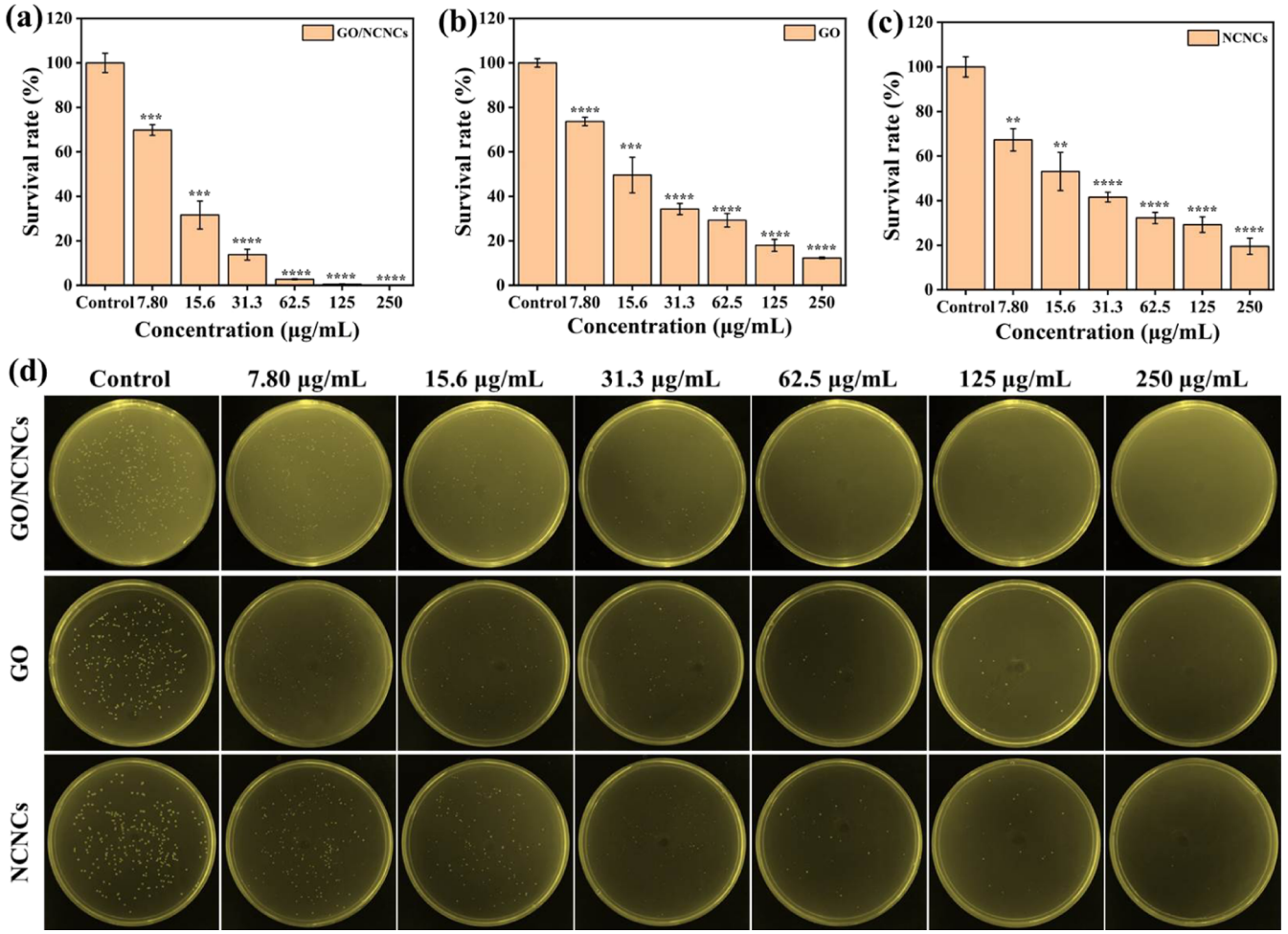

Figure 4. Dose−response to the survival rate of *S. aureus*. The survival rate of *S. aureus* treated with GO/NCNCs (a), GO (b), and NCNCs (c). Photographs of the agar plates of *S. aureus* exposed or unexposed to various concentrations of GO/NCNCs, GO, and NCNCs (7.80−250 μg/mL) (d).

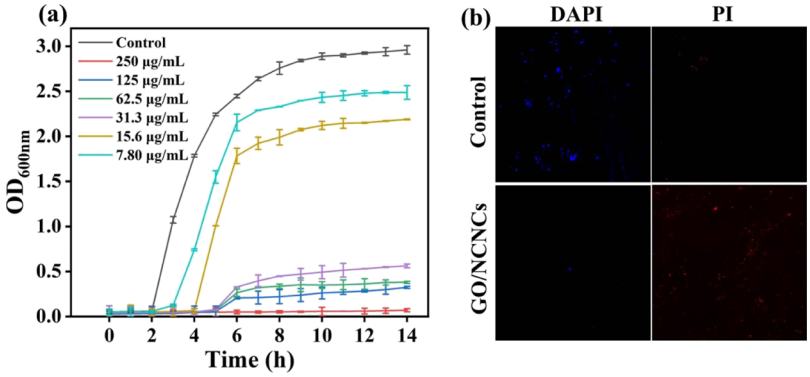

Figure 5. Growth curve of *S. aureus* cultured with various concentrations of GO/NCNCs (a) and fluorescence microscopy images of *S. aureus* stained with PI and DAPI after exposure to 125 μg/mL GO/NCNCs or PBS (b).

to be encapsulated by the GO sheet, which will disrupt the integrity of the pathogen's plasma membrane through physical damage.[38] The dispersion of NCNCs into the bacterial suspension confirmed that NCNCs can bind and capture bacteria by interacting with specific components at the bacterial surface, implicating that synergistic antibacterial advantages can be achieved by assembling GO and NCNCs into nanocomposites. To verify whether GO/NCNCs have a stronger ability to capture and destroy the cell membrane, the morphology of *S. aureus* was observed by TEM. As illustrated in Figure 6a, the *S. aureus* cells in the control group presented a representative spherical shape, with a smooth and intact membrane. After exposure to 125 μg/mL GO, the *S. aureus* cells were wrapped by the thin sheets of GO, causing the cells to deform and collapse (Figure 6b). In Figure 6c, the NCNCs are seen to have bound to the surface of *S. aureus* cells, causing the cells to deform obviously, while in Figure 6d, the GO/NCNC nanocomposite is shown to cause severe damage to the

https://doi.org/10.1021/acsomega.2c00508
ACS Omega 2022, 7, 18339−18349

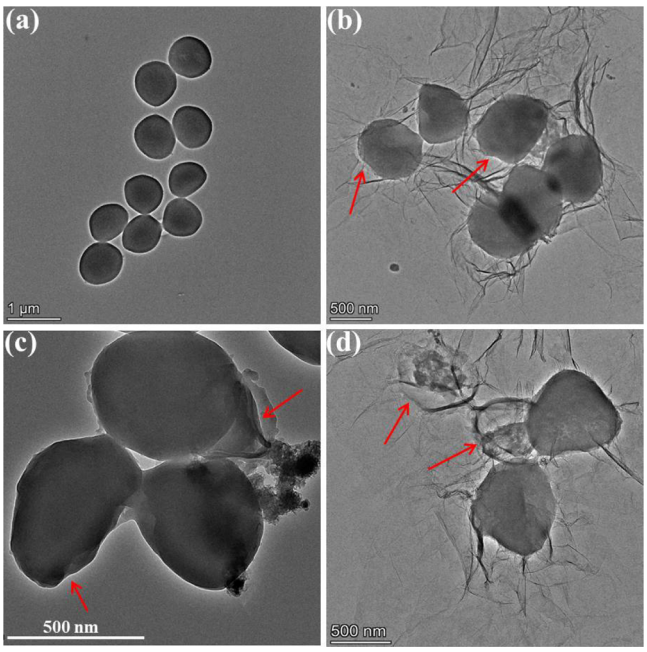

Figure 6. TEM images of *S. aureus* unexposed (a) or exposed to 125 μg/mL GO (b), NCNCs (c), or GO/NCNCs (d).

cell membrane, and the intracellular contents were obviously leaked, indicating the strong antibacterial efficiency of the GO/NCNC nanocomposite, which can be ascribed to the synergistic effect between GO and NCNCs.

SEM further verified the morphological changes of *S. aureus*. As shown in Figure 7a, the *S. aureus* cells in the control group

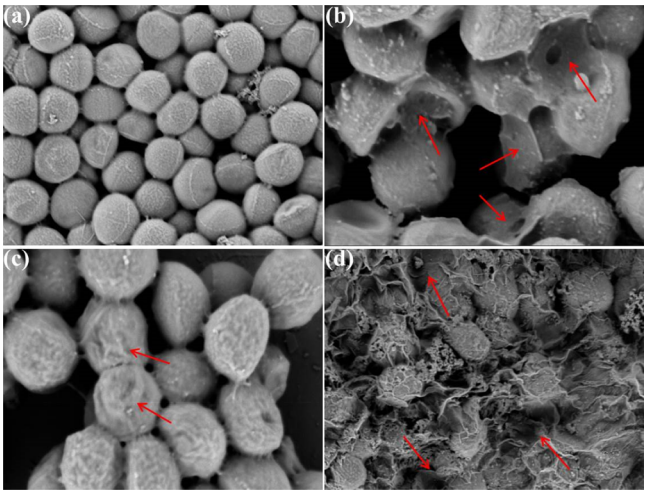

Figure 7. SEM images of *S. aureus* cells untreated (a) or treated with 125 μg/mL GO (b), NCNCs (c), and GO/NCNCs (d).

presented a rod shape with smooth cell walls, indicating that the cells were in a healthy state. However, the GO treatment severely damaged the structure of the bacterial walls (Figure 7b), the NCNC treatment caused lots of wrinkles on the cell wall surface (Figure 7c), and the exposure of *S. aureus* to GO/NCNCs largely destroyed the structure of *S. aureus* cells, causing them to lose their original shape and become fragmented (Figure 7d). These results were consistent with the conclusion of a previous report that indicated that the adsorption of nanoparticles on the bacterial cell wall is responsible for the bactericidal effect of nanomaterial interactions with biological cells. Due to its rich oxygen-containing groups, GO can form hydrogen bonds with lipopolysaccharide subunits containing sugars, phosphates, and lipids in cell membranes.[39] The TEM and SEM results are consistent with the plate coating results, indicating the strong synergistic antibacterial ability of the GO/NCNC nanocomposite. Xie et al. fabricated GO/AgNP/collagen hybrid coatings. The coating showed higher antibacterial activity than pure AgNPs and GO due to AgNP-GO particle release of Ag^+ and visible light-induced ROS generation.[40] With the same synergistic antibacterial strategy, the polyurethane/siloxane network containing GO nanosheets prepared by Shams et al. through the sol−gel hydrolysis/condensation process can achieve an extensive synergistic antibacterial effect against fungi and Gram-positive/-negative bacteria.[41]

3.4.2. Leaching of Ni^{2+}. The leach of Ni^{2+} during the co-incubation of GO/NCNCs with bacteria was confirmed by quantifying the amount of Ni^{2+} in bacterial solutions treated with GO/NCNCs at different incubation time intervals using inductively coupled plasma mass spectrometry. As shown in Figure S5, with the increase in incubation time, the leach of Ni^{2+} in the 125 μg/mL GO/NCNC treatment group gradually increased, and the leach amount was in the range of 0.34−0.60 μg/mL. To verify whether leached Ni^{2+} has antibacterial activity, the inhibitory effects of different concentrations of Ni^{2+} (0.2, 0.4, and 0.6 μg/mL) on *S. aureus* and *E. coli* were evaluated by agar plate experiments. As displayed in Figure S6, different concentrations of Ni^{2+} had certain inhibitory effects on *S. aureus* and *E. coli*. When the concentration reached 0.6 μg/mL, the inhibition rates of *S. aureus* and *E. coli* were 43.7 and 83.6%, respectively, indicating that leaching Ni^{2+} plays a certain role in the antibacterial effect of the GO/NCNCs.

3.4.3. Overexpression of ROS. The endogenously generated ROS plays a key role in signal transduction, but the ROS level exceeding the cell elimination ability will trigger a chain reaction, leading to the breaking of DNA, proteins, lipids, and other biological macromolecules.[42,43] Therefore, destruction of bacterial walls and cell membranes is probably not the only effective mechanism for bacterial death, and GO/NCNCs may also kill bacterial cells by regulating ROS production. To test this hypothesis, we detected the production of ROS under GO, NCNC, and GO/NCNC exposure through the fluorescent probe DCFH-DA, which diffuses passively into cells through the cell membrane. As shown in Figure 8a−d, the green fluorescence intensity of *S. aureus* cells exposed to GO, NCNCs, or GO/NCNCs was higher than that of the control group. Meanwhile, the treatment with GO or NCNCs exhibited only a small amount of the fluorescent signal, in contrast to strong fluorescent signals in the presence of the GO/NCNC nanocomposite. These results confirmed that the GO/NCNC nanocomposite could induce intracellular ROS production in bacteria, which may account for its antibacterial effects. To date, possible antibacterial mechanisms of GO-based nanomaterials have been demonstrated, including cell membrane stress caused by mechanical damage of GO nanosheets and oxidative stress associated with cellular ROS production.[44] ROS mainly include the free radicals of superoxide anions ($^{\bullet}O_2^-$), hydroxyl radicals ($^{\bullet}OH$), and H_2O_2, which are commonly regarded as the main active substances for sterilization. In the present study, the $^{\bullet}OH$ and $^{\bullet}O_2^-$ radicals induced by the GO/NCNC nanocomposite were measured by the electron spin resonance-5,5-dimethyl-1-

https://doi.org/10.1021/acsomega.2c00508
ACS Omega 2022, 7, 18339−18349

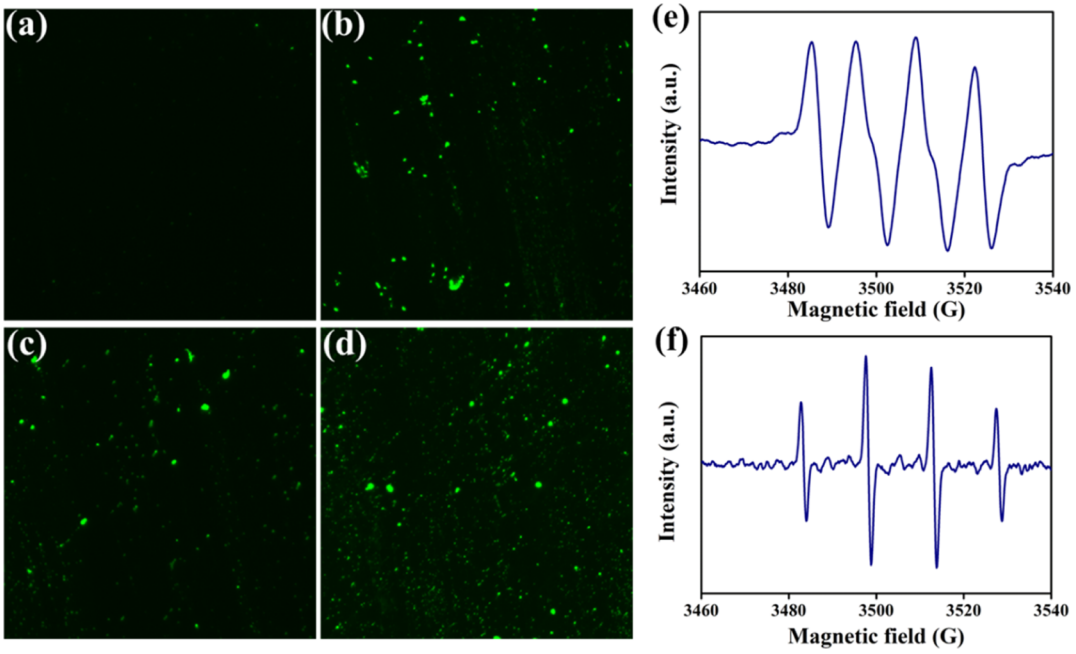

Figure 8. ROS production in *S. aureus* cells detected by DCFH-DA staining. Fluorescence microscope images of *S. aureus* cells untreated (a) or treated with GO (b), NCNCs (c), and GO/NCNCs (d). ESR images of DMPO−$^{\bullet}$OH (e) and DMPO−$^{\bullet}O_2^-$(f) for the GO/NCNC nanocomposite.

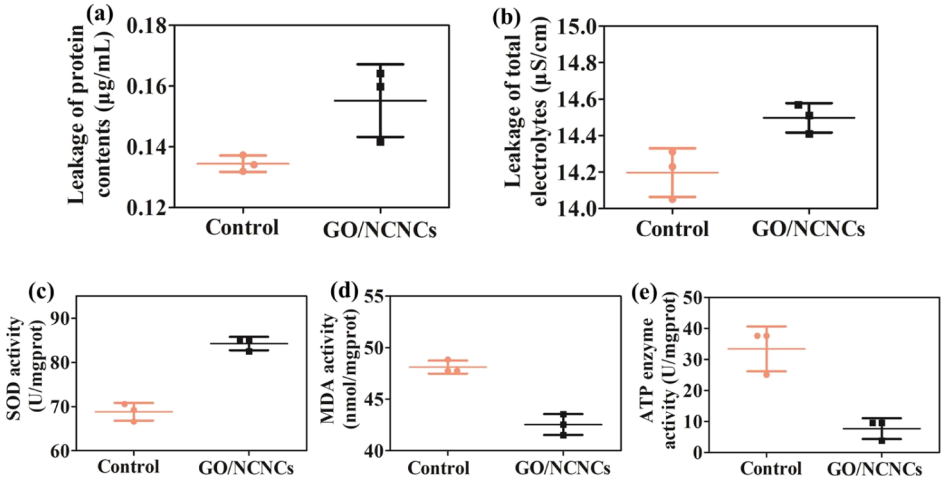

Figure 9. Total protein content (a), total electrolyte (b), SOD activity (c), MDA activity (d), and ATPase activity (e) in *S. aureus* cells after exposure to 125 μg/mL GO/NCNCs. * and ** indicate $p < 0.05$ and <0.01 compared with the control cells, respectively.

pyrroline-N-oxide (ESR-DMPO) method. In Figure 8e,f, the typical $^{\bullet}$OH/DMPO and $^{\bullet}O_2^-$/DMPO peaks can be observed, indicating the potential participation of $^{\bullet}O_2^-$ and $^{\bullet}$OH in sterilization. Many studies have shown that the excessive ROS induced by nanomaterials will assault DNA macromolecules, promote the damage of the bacterial wall structure, and ultimately cause bacterial death.[45] Zhang et al. synthesized a novel antibacterial copper cluster (CuC) molecule and found that CuCs can trigger the massive production of ROS in bacteria, and the overloaded endogenous ROS can accelerate bacterial wall rupture, resulting in bacterial death.[46]

When the structure integrity of bacteria is damaged, the intercellular components, including ions, DNA, electrolytes, and proteins, will leak out. A microplate reader and a conductivity meter were used to quantify the concentration of extracellular proteins and electrolytes after GO/NCNC treatment. As illustrated in Figure 9a,b, compared with the untreated control group, the GO/NCNC group showed a significant increase in the leakage of the protein content ($p < 0.05$) and total electrolyte ($p < 0.01$) in the *S. aureus* cells. Additionally, the damaged cell membrane of *S. aureus* was examined by measuring the superoxide dismutase (SOD), ATPase, and malondialdehyde (MDA) activity after exposure to GO/NCNCs. In Figure 9c, the SOD level is seen to increase significantly ($p < 0.01$) from 68.8 to 84.3 U/mg$_{prot}$ after the treatment with 125 μg/mL GO/NCNCs. Adenosine triphosphate (ATP), one of the most crucial energy-related molecules in bacteria, is essential for the cell function, growth, and survival of microorganisms, and its concentration is a vital index for microbial available energy. The ATP activity of *S. aureus* treated with 125 μg/mL GO/NCNCs showed 4.4-fold reduction when compared to the control group (Figure 9e).

https://doi.org/10.1021/acsomega.2c00508
ACS Omega 2022, 7, 18339−18349

Meanwhile, the MDA activity significantly ($p < 0.05$) decreased from 48.1 to 42.5 nmol/mg_{prot} in response to 125 μg/mL treatment (Figure 9d). These results demonstrated that the GO/NCNC nanocomposite could destroy the bacterial wall and membrane and induce the leakage of intracellular components, for instance, proteins and electrolytes, further supporting the conclusions of TEM and SEM. Previous studies have attributed the observed decrease in the intracellular ATP concentration to the rapid hydrolysis of ATP or the leakage of intracellular ATP from the cell membrane due to the change of cell membrane permeability.[47] Recent studies have also shown that once the bacterial membrane is damaged, substances such as ATP and proteins will be excreted outside the cell.[48,49] Xie et al. proposed a synergistic antibacterial system based on copper peroxide-supported tungsten disulfide nanoflowers (CP@WS_2 NFs), which resulted in severe leakage of cellular components and reduced the amount of ATP and disrupted bacterial membranes.[50]

4. CONCLUSIONS

In summary, a novel, biocompatible, and synergistic antibacterial nanocomposite, GO/NCNCs, was constructed via the simple electrostatic assembly of NCNCs with GO sheets, and its properties were characterized using various analytical techniques. *In vitro* antibacterial experiments demonstrated that at a concentration of 125 μg/mL, the GO/NCNC nanocomposite showed better antibacterial properties than pure GO and NCNCs, with an antibacterial efficiency of 99.5 and 100% against *S. aureus* and *E. coli, respectively*. SEM, TEM, and ROS analyses showed that the synergistic effect of GO and NCNCs played a crucial role in the inactivation of *S. aureus* cells, with NCNCs binding and capturing bacteria and GO causing irreversible physical damage to the biological structure of bacteria. Additionally, the synergistic effects can also induce stronger oxidative stress in cells, resulting in more serious damage to the membrane, changes in bacterial metabolic enzyme activity, and leakage of intracellular contents and eventually bacterial death. The leaching of Ni^{2+} during the interaction between GO/NCNCs and bacteria is also responsible for the antibacterial effect. Future studies can focus on the pharmacodynamics and toxicology of the GO/NCNC nanocomposite with appropriate animal models. The overall results imply that the GO/NCNC nanocomposite is a hopeful antimicrobial agent.

■ ASSOCIATED CONTENT

Supporting Information

The Supporting Information is available free of charge at https://pubs.acs.org/doi/10.1021/acsomega.2c00508.

Magnetic hysteresis loop and magnetic enrichment of the GO/NCNC nanocomposite; XPS characterization of GO; XPS characterization of NCNCs; dose−response to the survival rate of *E. coli*; leach of Ni^{2+} measured at different incubation time intervals under the treatment of the 125 μg/mL GO/NCNCs; survival rates of *S. aureus* (a) and *E. coli* (b) treated with different concentrations of Ni^{2+} and the corresponding pictures of colonies formed by *S. aureus* (c) and *E. coli* (d) under the treatment of Ni^{2+} at different concentrations (PDF)

■ AUTHOR INFORMATION

Corresponding Authors

Xinjun Du − *State Key Laboratory of Food Nutrition and Safety, Key Laboratory of Food Nutrition and Safety, Ministry of Education, College of Food Science and Engineering, Tianjin University of Science and Technology, Tianjin 300457, PR China;* orcid.org/0000-0003-3454-990X; Email: xjdu@tust.edu.cn

Shuo Wang − *Tianjin Key Laboratory of Food Science and Health, School of Medicine, Nankai University, Tianjin 300071, PR China;* orcid.org/0000-0003-0910-6146; Email: wangshuo@nankai.edu.cn

Authors

Ting Du − *State Key Laboratory of Food Nutrition and Safety, Key Laboratory of Food Nutrition and Safety, Ministry of Education, College of Food Science and Engineering, Tianjin University of Science and Technology, Tianjin 300457, PR China;* orcid.org/0000-0002-8980-9038

Baojia Huang − *State Key Laboratory of Food Nutrition and Safety, Key Laboratory of Food Nutrition and Safety, Ministry of Education, College of Food Science and Engineering, Tianjin University of Science and Technology, Tianjin 300457, PR China*

Jiangli Cao − *State Key Laboratory of Food Nutrition and Safety, Key Laboratory of Food Nutrition and Safety, Ministry of Education, College of Food Science and Engineering, Tianjin University of Science and Technology, Tianjin 300457, PR China*

Chunqiao Li − *State Key Laboratory of Food Nutrition and Safety, Key Laboratory of Food Nutrition and Safety, Ministry of Education, College of Food Science and Engineering, Tianjin University of Science and Technology, Tianjin 300457, PR China*

Jingbo Jiao − *State Key Laboratory of Food Nutrition and Safety, Key Laboratory of Food Nutrition and Safety, Ministry of Education, College of Food Science and Engineering, Tianjin University of Science and Technology, Tianjin 300457, PR China*

Zehui Xiao − *State Key Laboratory of Food Nutrition and Safety, Key Laboratory of Food Nutrition and Safety, Ministry of Education, College of Food Science and Engineering, Tianjin University of Science and Technology, Tianjin 300457, PR China*

Lifei Wei − *State Key Laboratory of Food Nutrition and Safety, Key Laboratory of Food Nutrition and Safety, Ministry of Education, College of Food Science and Engineering, Tianjin University of Science and Technology, Tianjin 300457, PR China*

Jing Ma − *College of Life Science, Yangtze University, Jingzhou 434023 Hubei, PR China*

Complete contact information is available at: https://pubs.acs.org/10.1021/acsomega.2c00508

Author Contributions

[‖]T.D. and B.H. contributed equally to this work.

Notes

The authors declare no competing financial interest.

■ ACKNOWLEDGMENTS

This work was supported by the National Natural Science Foundation of China (31972167 and 31902304), the Natural

Science Foundation of Tianjin (20JCQNJC00140), the National Key R & D Program (2018YFC1603800), the Key Laboratory of Food Nutrition and Safety, Ministry of Education, and Tianjin Key Laboratory of Food Nutrition and Safety, Tianjin University of Science and Technology, Tianjin, 300457, P. R. China (TJS201901).

REFERENCES

(1) Blaser, M. J. Antibiotic use and its consequences for the normal microbiome. *Science* **2016**, *352*, 544−545.
(2) Flemming, H.; Wingender, J. The biofilm matrix. *Nat. Rev. Microbiol.* **2010**, *8*, 623−633.
(3) Smith, A. Biofilms and antibiotic therapy: Is there a role for combating bacterial resistance by the use of novel drug delivery systems? *Adv. Drug Delivery Rev.* **2005**, *57*, 1539−1550.
(4) Zhang, Y.; Sun, P.; Zhang, L.; Wang, Z.; Wang, F.; Dong, K.; Liu, Z.; Ren, J.; Qu, X. Silver-infused porphyrinic metal-organic framework: Surface-adaptive, on-demand nanoplatform for synergistic bacteria killing and wound disinfection. *Adv. Funct. Mater.* **2019**, *29*, 1808594.
(5) Zhu, M.; Liu, X.; Tan, L.; Cui, Z.; Liang, Y.; Li, Z.; Kwok Yeung, K. W.; Wu, S. Photo-responsive chitosan/Ag/MoS_2 for rapid bacteria-killing. *J. Hazard. Mater.* **2020**, *383*, 121122.
(6) Hu, D.; Li, H.; Wang, B.; Ye, Z.; Lei, W.; Jia, F.; Jin, Q.; Ren, K.-F.; Ji, J. Surface-adaptive gold nanoparticles with effective adherence and enhanced photothermal ablation of methicillin-resistant Staphylococcus aureus biofilm. *ACS Nano* **2017**, *11*, 9330−9339.
(7) Wang, H.; Zhang, J.; Song, Z.; Mu, Y.; Foda, M. F.; Wu, Y.; Han, H. An intelligent platform based on acidity-triggered aggregation of gold nanoparticles for precise photothermal ablation of focal bacterial infection. *Chem. Eng. J.* **2021**, *407*, 127076.
(8) Ermini, M. L.; Voliani, V. Antimicrobial nano-agents: The copper age. *ACS Nano* **2021**, *15*, 6008−6029.
(9) Xi, J.; Wei, G.; An, L.; Xu, Z.; Xu, Z.; Fan, L.; Gao, L. Copper/Carbon hybrid nanozyme: Tuning catalytic activity by the copper state for antibacterial therapy. *Nano Lett.* **2019**, *19*, 7645−7654.
(10) Xin, Q.; Shah, H.; Nawaz, A.; Xie, W.; Akram, M. Z.; Batool, A.; Tian, L.; Jan, S. U.; Boddula, R.; Guo, B.; Liu, Q.; Gong, J. R. Antibacterial carbon-based nanomaterials. *Adv. Mater.* **2019**, *31*, 1804838.
(11) Alavi, M.; Jabari, E.; Jabbari, E. Functionalized carbon-based nanomaterials and quantum dots with antibacterial activity: a review. *Expert Rev. Anti-Infect. Ther.* **2021**, *19*, 35−44.
(12) Liu, R.; Chen, X.; Chakraborty, S.; Lemke, J. J.; Hayouka, Z.; Chow, C.; Welch, R. A.; Weisblum, B.; Masters, K. S.; Gellman, S. H. Tuning the biological activity profile of antibacterial polymers via subunit substitution pattern. *J. Am. Chem. Soc.* **2014**, *136*, 4410−4418.
(13) Li, P.; Zhou, C.; Rayatpisheh, S.; Ye, K.; Poon, Y. F.; Hammond, P. T.; Duan, H.; Chan-Park, M. B. Cationic peptidopolysaccharides show excellent broad-spectrum antimicrobial activities and high selectivity. *Adv. Mater.* **2012**, *24*, 4130−4137.
(14) Yu, Q.; Deng, T.; Lin, F.-C.; Zhang, B.; Zink, J. I. Supramolecular assemblies of heterogeneous mesoporous silica nanoparticles to co-deliver antimicrobial peptides and antibiotics for synergistic eradication of pathogenic biofilms. *ACS Nano* **2020**, *14*, 5926−5937.
(15) Liu, Y.; Li, F.; Guo, Z.; Xiao, Y.; Zhang, Y.; Sun, X.; Zhe, T.; Cao, Y.; Wang, L.; Lu, Q.; Wang, J. Silver nanoparticle-embedded hydrogel as a photothermal platform for combating bacterial infections. *Chem. Eng. J.* **2020**, *382*, 122990.
(16) Liu, H.; Zhu, X.; Guo, H.; Huang, H.; Huang, S.; Huang, S.; Xue, W.; Zhu, P.; Guo, R. Nitric oxide released injectable hydrogel combined with synergistic photothermal therapy for antibacterial and accelerated wound healing. *Appl. Mater. Today* **2020**, *20*, 100781.
(17) Afewerki, S.; Wang, X.; Ruiz-Esparza, G. U.; Tai, C.-W.; Kong, X.; Zhou, S.; Welch, K.; Huang, P.; Bengtsson, R.; Xu, C.; Strømme, M. Combined catalysis for engineering bioinspired, lignin-based, long-lasting, adhesive, self-mending, antimicrobial hydrogels. *ACS Nano* **2020**, *14*, 17004−17017.
(18) Lu, A.-H.; Salabas, E. L.; Schüth, F. Magnetic nanoparticles: Synthesis, protection, functionalization, and application. *Angew. Chem., Int. Ed.* **2007**, *46*, 1222−1244.
(19) Taylor, E. N.; Kummer, K. M.; Durmus, N. G.; Leuba, K.; Tarquinio, K. M.; Webster, T. J. Superparamagnetic iron oxide nanoparticles (SPION) for the treatment of antibiotic-resistant biofilms. *Small* **2012**, *8*, 3016−3027.
(20) Sharma, V. K.; McDonald, T. J.; Kim, H.; Garg, V. K. Magnetic graphene-carbon nanotube iron nanocomposites as adsorbents and antibacterial agents for water purification. *Adv. Colloid Interface Sci.* **2015**, *225*, 229−240.
(21) Liu, Y.; Guo, Z.; Li, F.; Xiao, Y.; Zhang, Y.; Bu, T.; Jia, P.; Zhe, T.; Wang, L. Multifunctional magnetic copper ferrite nanoparticles as fenton-like reaction and near-infrared photothermal agents for synergetic antibacterial therapy. *ACS Appl. Mater. Interfaces* **2019**, *11*, 31649−31660.
(22) El-Boubbou, K.; Gruden, C.; Huang, X. Magnetic glyco-nanoparticles: A unique tool for rapid pathogen detection, decontamination, and strain differentiation. *J. Am. Chem. Soc.* **2007**, *129*, 13392−13393.
(23) Peng, B.; Zhang, X.; Aarts, D. G. A. L.; Dullens, R. P. A. Superparamagnetic nickel colloidal nanocrystal clusters with antibacterial activity and bacteria binding ability. *Nat. Nanotechnol.* **2018**, *13*, 478−482.
(24) Natan, M.; Edin, F.; Perkas, N.; Yacobi, G.; Perelshtein, I.; Segal, E.; Homsy, A.; Laux, E.; Keppner, H.; Rask-Andersen, H.; Gedanken, A.; Banin, E. Two are better than one: Combining ZnO and MgF_2 nanoparticles reduces streptococcus pneumoniae and Staphylococcus aureus biofilm formation on cochlear implants. *Adv. Funct. Mater.* **2016**, *26*, 2473−2481.
(25) Sharma, D.; Kanchi, S.; Sabela, M. I.; Bisetty, K. Insight into the biosensing of graphene oxide: Present and future prospects. *Arabian J. Chem.* **2016**, *9*, 238−261.
(26) Li, X.; Rui, M.; Song, J.; Shen, Z.; Zeng, H. Carbon and graphene quantum dots for optoelectronic and energy devices: A review. *Adv. Funct. Mater.* **2015**, *25*, 4929−4947.
(27) Karahan, H. E.; Wiraja, C.; Xu, C. J.; Wei, J.; Wang, Y. L.; Wang, L.; Liu, F.; Chen, Y. Graphene materials in antimicrobial nanomedicine: Current status and future perspectives. *Adv. Healthcare Mater.* **2018**, *7*, No. e1701406.
(28) Chen, J.; Peng, H.; Wang, X.; Shao, F.; Yuan, Z.; Han, H. Graphene oxide exhibits broad-spectrum antimicrobial activity against bacterial phytopathogens and fungal conidia by intertwining and membrane perturbation. *Nanoscale* **2014**, *6*, 1879−1889.
(29) Chen, J.; Sun, L.; Cheng, Y.; Lu, Z.; Shao, K.; Li, T.; Hu, C.; Han, H. Graphene oxide-silver nanocomposite: Novel agricultural antifungal agent against fusarium graminearum for crop disease prevention. *ACS Appl. Mater. Interfaces* **2016**, *8*, 24057−24070.
(30) Liang, Y.; Wang, M.; Zhang, Z.; Ren, G.; Liu, Y.; Wu, S.; Shen, J. Facile synthesis of ZnO QDs@GO-CS hydrogel for synergetic antibacterial applications and enhanced wound healing. *Chem. Eng. J.* **2019**, *378*, 122043.
(31) Ye, S.; Shao, K.; Li, Z.; Guo, N.; Zuo, Y.; Li, Q.; Lu, Z.; Chen, L.; He, Q.; Han, H. Antiviral activity of graphene oxide: How sharp edged structure and charge matter. *ACS Appl. Mater. Interfaces* **2015**, *7*, 21571−21579.
(32) Xu, Y.; Bai, H.; Lu, G.; Li, C.; Shi, G. Flexible graphene films via the filtration of water-soluble noncovalent functionalized graphene sheets. *J. Am. Chem. Soc.* **2008**, *130*, 5856−5857.
(33) Sun, L.; Du, T.; Hu, C.; Chen, J.; Lu, J.; Lu, Z.; Han, H. Antibacterial activity of graphene oxide/g-C_3N_4 composite through photocatalytic disinfection under visible light. *ACS Sustainable Chem. Eng.* **2017**, *5*, 8693−8701.
(34) Du, T.; Liang, J.; Dong, N.; Liu, L.; Fang, L.; Xiao, S.; Han, H. Carbon dots as inhibitors of virus by activation of type I interferon response. *Carbon* **2016**, *110*, 278−285.

https://doi.org/10.1021/acsomega.2c00508
ACS Omega 2022, 7, 18339−18349

(35) Karahan, H. E.; Wei, L.; Goh, K.; Wiraja, C.; Liu, Z.; Xu, C.; Jiang, R.; Wei, J.; Chen, Y. Synergism of water shock and a biocompatible block copolymer potentiates the antibacterial activity of graphene oxide. *Small* **2016**, *12*, 951−962.
(36) Zhao, R.; Lv, M.; Li, Y.; Sun, M.; Kong, W.; Wang, L.; Song, S.; Fan, C.; Jia, L.; Qiu, S.; Sun, Y.; Song, H.; Hao, R. Stable nanocomposite based on PEGylated and silver nanoparticles loaded graphene oxide for long-term antibacterial activity. *ACS Appl. Mater. Interfaces* **2017**, *9*, 15328−15341.
(37) Gao, Y.; Wu, J.; Ren, X.; Tan, X.; Hayat, T.; Alsaedi, A.; Cheng, C.; Chen, C. Impact of graphene oxide on the antibacterial activity of antibiotics against bacteria. *Environ. Sci.: Nano* **2017**, *4*, 1016−1024.
(38) Liu, S.; Zeng, T. H.; Hofmann, M.; Burcombe, E.; Wei, J.; Jiang, R.; Kong, J.; Chen, Y. Antibacterial activity of graphite, graphite oxide, graphene oxide, and reduced graphene oxide: membrane and oxidative stress. *ACS Nano* **2011**, *5*, 6971−6980.
(39) Elahifard, M. R.; Rahimnejad, S.; Haghighi, S.; Gholami, M. R. Apatite-coated Ag/AgBr/TiO_2 visible-light photocatalyst for destruction of bacteria. *J. Am. Chem. Soc.* **2007**, *129*, 9552−9553.
(40) Xie, X.; Mao, C.; Liu, X.; Zhang, Y.; Cui, Z.; Yang, X.; Yeung, K. W. K.; Pan, H.; Chu, P. K.; Wu, S. Synergistic bacteria killing through photodynamic and physical actions of graphene oxide/Ag/collagen coating. *ACS Appl. Mater. Interfaces* **2017**, *9*, 26417−26428.
(41) Shams, E.; Yeganeh, H.; Naderi-Manesh, H.; Gharibi, R.; Mohammad Hassan, Z. Polyurethane/siloxane membranes containing graphene oxide nanoplatelets as antimicrobial wound dressings: in vitro and in vivo evaluations. *J. Mater. Sci.: Mater. Med.* **2017**, *28*, 75.
(42) AshaRani, P. V.; Low Kah Mun, G.; Hande, M. P.; Valiyaveettil, S. Cytotoxicity and genotoxicity of silver nanoparticles in human cells. *ACS Nano* **2009**, *3*, 279−290.
(43) Song, Z.; Wu, Y.; Wang, H.; Han, H. Synergistic antibacterial effects of curcumin modified silver nanoparticles through ROS-mediated pathways. *Mater. Sci. Eng., C* **2019**, *99*, 255−263.
(44) Akhavan, O.; Ghaderi, E.; Rahighi, R. Toward single-DNA electrochemical biosensing by graphene nanowalls. *ACS Nano* **2012**, *6*, 2904−2916.
(45) Zhao, H.; Huang, J.; Li, Y.; Lv, X.; Zhou, H.; Wang, H.; Xu, Y.; Wang, C.; Wang, J.; Liu, Z. ROS-scavenging hydrogel to promote healing of bacteria infected diabetic wounds. *Biomaterials* **2020**, *258*, 120286.
(46) Zhang, X.; Zhang, Z.; Shu, Q.; Xu, C.; Zheng, Q.; Guo, Z.; Wang, C.; Hao, Z.; Liu, X.; Wang, G.; Yan, W.; Chen, H.; Lu, C. Copper clusters: An effective antibacterial for eradicating multidrug-resistant bacterial infection in vitro and in vivo. *Adv. Funct. Mater.* **2021**, *31*, 2008720.
(47) Mempin, R.; Tran, H.; Chen, C.; Gong, H.; Kim Ho, K.; Lu, S. Release of extracellular ATP by bacteria during growth. *BMC Microbiol.* **2013**, *13*, 301.
(48) Yu, S.; Li, G.; Liu, R.; Ma, D.; Xue, W. Dendritic Fe_3O_4@Poly(dopamine)@PAMAM nanocomposite as controllable NO-releasing material: A synergistic photothermal and NO antibacterial study. *Adv. Funct. Mater.* **2018**, *28*, 1707440.
(49) Cao, B.; Xiao, F.; Xing, D.; Hu, X. Polyprodrug antimicrobials: Remarkable membrane damage and concurrent drug release to combat antibiotic resistance of methicillin-resistant staphylococcus aureus. *Small* **2018**, *14*, 1802008.
(50) Xie, X.; Wang, R.; Zhang, X.; Ren, Y.; Du, T.; Ni, Y.; Yan, H.; Zhang, L.; Sun, J.; Zhang, W.; Wang, J. A photothermal and self-induced fenton dual-modal antibacterial platform for synergistic enhanced bacterial elimination. *Appl. Catal., B* **2021**, *295*, 120315.

https://doi.org/10.1021/acsomega.2c00508
ACS Omega 2022, 7, 18339−18349